Superconducting properties of NbN film, bridge and meanders

Lalit M. Joshi, Apoorva Verma, Anurag Gupta, P. K. Rout, Sudhir Husale, and R. C. Budhani

Citation: AIP Advances **8**, 055305 (2018); doi: 10.1063/1.5026219
View online: https://doi.org/10.1063/1.5026219
View Table of Contents: http://aip.scitation.org/toc/adv/8/5
Published by the American Institute of Physics

Superconducting properties of NbN film, bridge and meanders

Lalit M. Joshi,[1,2] Apoorva Verma,[1,2] Anurag Gupta,[1,2,a] P. K. Rout,[1] Sudhir Husale,[1,2] and R. C. Budhani[3]
[1]*CSIR-National Physical Laboratory, New Delhi, India*
[2]*Academy of Scientific and Innovative Research (AcSIR), CSIR-NPL, New Delhi, India*
[3]*Condensed Matter-Low Dimensional Systems Laboratory, Indian Institute of Technology, Kanpur, India*

(Received 16 February 2018; accepted 18 April 2018; published online 3 May 2018)

The transport properties of superconducting NbN nanostructures in the form of thin film, bridge of width (w) = 50 μm and three meanders of w = 500, 250 and 100 nm have been investigated by resistance (R) measurements in temperature (T) range = 2 -300 K and magnetic field (B) range = 0 - 7 Tesla. The nanostructuring was carried out using Focused Ion Beam (FIB) milling. Reduction of sample width results in significant changes in the normal and superconducting state properties. For instance, the observed metallic behavior in the thin film sample is lost and the normal state resistance increases drastically from 2.4 Ω to 418 kΩ for the 100 nm meander. In the superconducting state, the value of critical temperature T_c (upper critical field B_{c2} at T = 0 K) reduces gradually with width reduction, it changes from 13.15 K (42.8 Tesla) in the case of thin film sample to 5.7 K (12.7 Tesla) for the 100 nm meander sample. The superconducting transitions are found to get broader for the bridge sample and the meanders additionally show low-temperature resistive tails. In case of all the samples with reduced width, the transition onsets are found to be rounded at surprisingly high values of $T \sim 25$ K >> T_c. These results are discussed in terms of the possible effects of FIB processing and weak localization in our samples. https://doi.org/10.1063/1.5026219

I. INTRODUCTION

Nb-based superconductors have been well known for many applications in bulk form and in nanostructured form as well.[1,2] In the latter case, various characteristics have been exploited to build superconducting electronic devices.[3] For instance, thin films of superconductors have been found to be ideal for devices like Transition Edge Sensor (TES), which utilises the property of high dR/dT of superconductors in transition regime;[4] superconducting loop with one or two Josephson junctions forms ultra-sensitive superconducting quantum interference devices which use quantum tunneling of electrons from weakly linked superconductors;[5] and the superconducting nanowire functioning as single photon detector has proven to be very promising for communication applications.[6,7] Several nanofabrication techniques like Pulse Laser Deposition, DC Sputtering, e-beam lithography and focused ion beam (FIB) milling are utilized to fabricate superconducting nanostructures.[5,8–10] It is well known that reduced dimensions of nanostructures can lead to radically different superconducting behavior [Ref. 11 and references therein]. In addition to the size effects, the nanofabrication process itself may also induce microstructural/chemical changes in the nanostructures.[12,13] Thus it becomes important to study and differentiate the two effects for the realization of devices with tailored properties.

[a]Electronic mail: anurag@nplindia.org

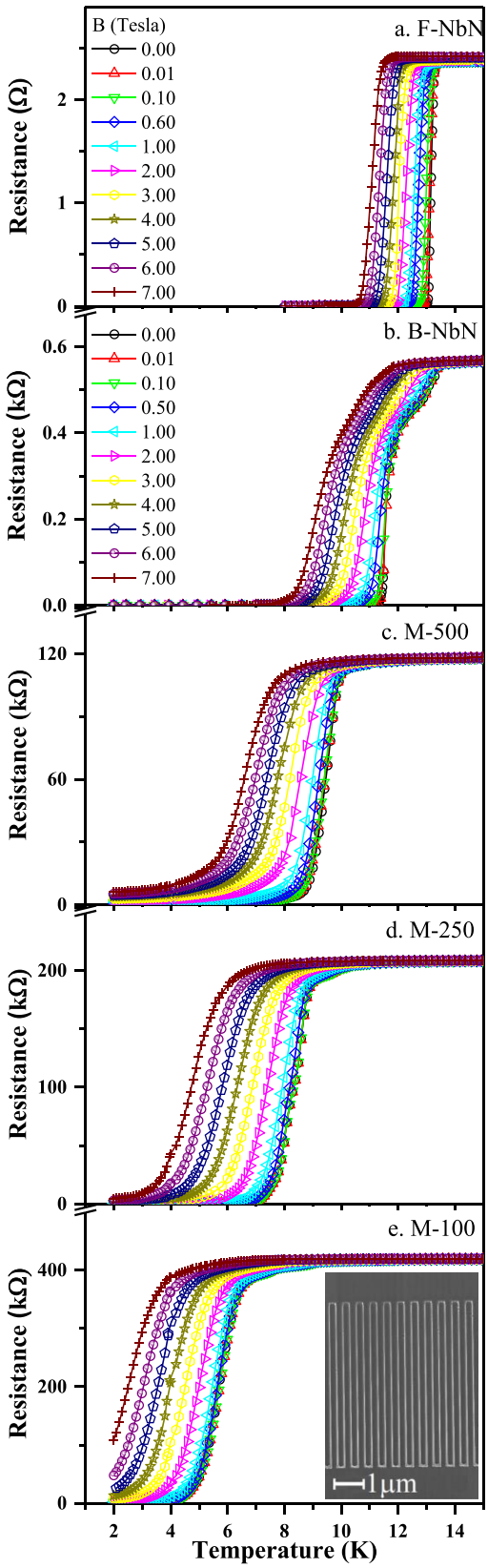

FIG. 1. Resistance as a function of temperature at various magnetic fields for F-NbN, B-NbN, M-500, M-250 and M-100 samples. The inset of 'e' shows SEM image of M-100 sample.

In the present work, we have attempted to address these issues through transport studies of NbN nanostructures, where a host NbN film of 50 nm thickness is gradually reduced by FIB milling to varying sample widths of 50 μm, 500 nm, 250 nm and 100 nm. The highlight of the present work is the observed scaling of both the normal and superconducting state properties of our nanostructures with width, which can be understood by the combined effect of width reduction and FIB induced microstructural changes.

II. EXPERIMENTAL DETAILS

NbN thin films of thickness 50 nm are deposited on Si/SiO_2 substrate using DC sputtering in $Ar–N_2$ pressure of 7.5E −3 mbar. The substrate temperature was kept at 200 °C during the growth of the thin films. Further, a bridge of width 50μm and three meanders of width 500, 250 and 100 nm are fabricated from the NbN thin film by focused Ga ion-beam (FIB) milling performed in an Auriga, Zeiss dual beam system with an accelerating voltage of 30 kV. The milling pattern of bridge and meander lines was optimized and milled at an ion beam current ~ 240 pA to obtain the required pattern. As an example, inset of Fig. 1(e) shows the SEM image of the meander sample with w = 100 nm. NbN film and bridge samples are denoted as F-NbN and B-NbN, and the meander samples are referred to as M-500, M-250, and M-100 based on their respective widths. The resistance as a function of temperature ($R(T)$) is measured for all the five samples in T range = 2 - 300 K and B range = 0 - 7 Tesla in four-probe geometry using an MPMS cryostat (Quantum Design). The accuracy of the temperature is better than ±25 mK below 50 K.

III. RESULTS AND DISCUSSION

Fig. 1 shows the superconducting transition as observed in $R(T)$ at different constant magnetic fields for all the five samples F-NbN, B-NbN, M-500, M-250, and M-100. It is seen that with the decrease in the sample width the electrical transport shows an interesting evolution in both the normal and superconducting states. We first discuss the normal state behavior of our samples in detail. The normal state resistance at T = 15 K (R_{15K}) changes drastically from 2.4 Ω to 418 kΩ with the reducing sample width, see Table I. To understand if this change in R_{15K} is due to reduced width, we consider the relation between the resistance and sample dimensions, which is given as $R = \rho\,(l/wd)$ (where ρ is resistivity, l is length and w is width and d is the thickness of the sample). Since d (~50 nm) is same for all the samples, the value of R_{15K} should depend on ρ_{15K} and l, w. The expected R_{15K} values due to change in the sample dimension, estimated by assuming ρ to be same as the parent film sample, are found to be 30-70 times lower than the measured values. This indicates that the significant increase observed in R_{15K} values cannot be understood purely by the reduced sample dimensions. Instead, this result reveals a fabrication induced contribution to the observed change in the normal state resistance.

There is also a pronounced change observed in the temperature dependence of the normal state resistance, which is depicted for the entire T range in Fig. 2 at zero-field for all the samples. As seen, the bridge/meander samples (B-NbN, M-500, M-250 and M-100) all show a non-metallic behavior in comparison to the host thin film sample (F-NbN) that follows a metallic behavior. The non-metallic

TABLE I. Sample width, resistance measured, resistance expected and best fitted weak localization parameters 'l_e', 'k_F', 'α' and 'p' for all the samples.

Sample	Width μm	Resistance (15 K) (Measured) Ω	Resistance (15 K) (Expected) Ω	l_e nm	k_F nm^{-1}	α m^{-1}K^{-p}	p	$k_F\,l_e$
F-NbN	1400	2.4	-					
B-NbN	50	567	16.8	0.098	23.88	84.22	2.72	2.34
M-500	0.5	117919	1623.7	0.315	8.68	35.73	2.59	2.73
M-250	0.25	208138	4623.7	0.273	10.787	56.02	2.425	2.94
M-100	0.1	418857	10815.7	0.224	13.24	55.16	2.46	2.96

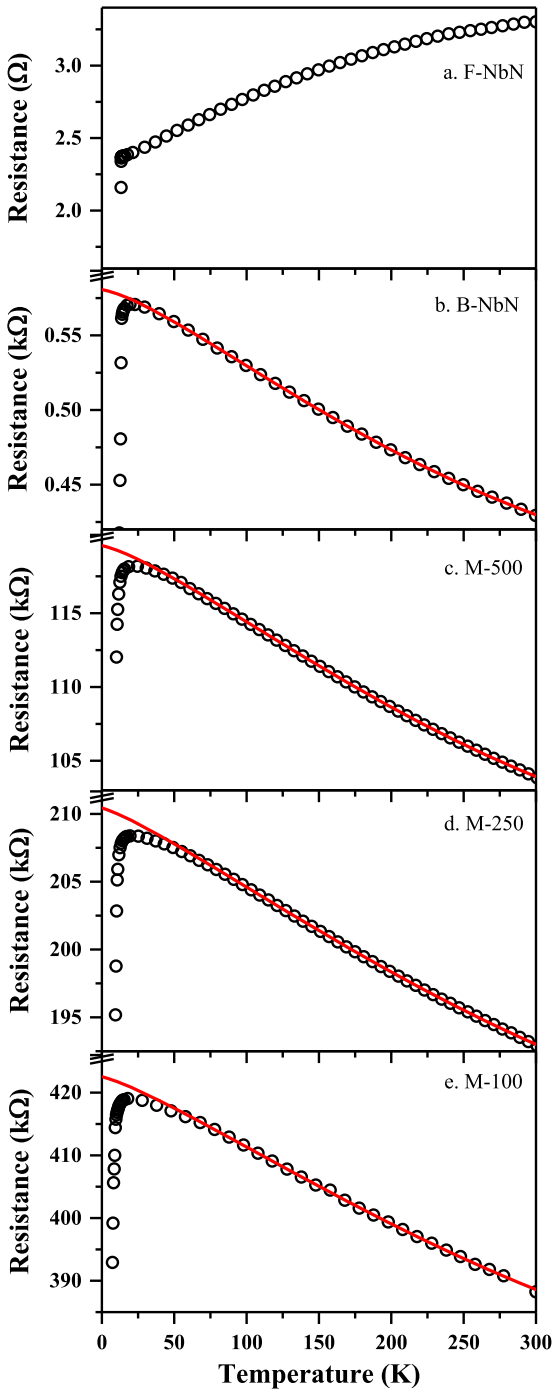

FIG. 2. Resistance as a function of temperature at $B = 0$ in the entire temperature range for F-NbN, B-NbN, M-500, M-250 and M-100 samples. The solid lines are theoretical fit, see text for details.

behavior has been reported earlier in polycrystalline[14–16] and epitaxial[17] NbN films. In case of epitaxial film this behavior has been discussed in terms of e^-- e^- interactions and weak localization whereas in polycrystalline samples, weak localization effects have been cited as the dominating reason behind the loss in metallic behavior. Since our samples are also polycrystalline, we apply the weak localization theory to understand our normal state $R(T)$ data. Weak localization arises as a consequence of quantum self-interference of electronic charge carriers and gives a negative contribution

to the electrical conductivity. As shown by Kaveh and Mott,[18] the expression for conductivity including both the Boltzmann conductivity and the conductivity arising due to weak localization can be approximated to,

$$\sigma = \sigma_B(0)\left(1 - \frac{3}{(k_F l_e)^2}\right) + \frac{e^2}{\pi^2\hbar}\left(\frac{1}{L_i} - \frac{(k_F l_e)^2}{3 l_i}\right) \quad (1)$$

where k_F *is* Fermi wave vector, l_e is elastic mean free path, l_i is inelastic mean free path, and L_i is the inelastic diffusion length given by, $L_i = \sqrt{\frac{1}{2} l_e l_i}$ The temperature dependence of conductivity comes from l_i whose variation with respect to temperature is given by a power law relation, $l_i^{-1} = \alpha T^p$ thus changing equation (1) to,

$$\sigma = \frac{1}{3\pi^2}\frac{e^2}{\hbar}\frac{1}{l_e}(k_F l_e)^2\left(1 - \frac{3}{(k_F l_e)^2}\right) + \frac{e^2}{\pi^2\hbar}\left(\sqrt{\frac{2\alpha}{l_e}T^p} - \alpha\frac{(k_F l_e)^2}{3}T^P\right) \quad (2)$$

Equation (2) was used to fit the observed $R(T)$ curves. The solid lines in Fig. 2 represent the best fit of the experimental data to equation (2) and are in excellent agreement, justifying the presence of weak localization in our samples. The values obtained for k_F, l_e, α and p are shown in Table I. For all the samples, $k_F l_e > 1$, that is one of the key conditions for observing weak localization. The observance of weak localization indicates a significant increase in disorder in our bridge and meander samples[18] in comparison to the thin film host sample, which is possibly a consequence of microstructural changes due to FIB. Note that the obtained values of the elastic mean free path (l_e) decrease with the reducing width of the meander samples barring the anomalous behavior of the B-NbN. As the elastic mean free path reduces the probability for intersecting electron paths increases exceptionally leading to a higher negative contribution to the conductivity and pronounced weak localization effects. This effect reflects as loss of metallic behavior and much higher resistances in case of our bridge and meander samples.

We now look in detail at the superconducting behavior of all the samples. From Fig. 1, it is observed that the superconducting transition shifts to lower temperatures as we decrease the width of the sample from F-NbN to M-100. The superconducting transition temperature (T_c) of each sample, defined at 50% of the transition, is tabulated in Table II.

Further, as expected, the transition is found to shift to lower temperatures with the increasing magnetic field for all the five samples. To quantify this shift, the upper critical fields (B_{c2}), defined at 50% of transition, are plotted as a function of temperature, as shown in Fig. 3.

As seen, the B_{c2} follows linear temperature dependence for all samples that is in agreement with the predictions of Ginzburg-Landau theory.[19] For all samples the linearly extrapolated values of $B_{c2}(0)$ at $T = 0$ K are shown in Table II. As was the case for T_c, $B_{c2}(0)$ also decreases with the width of the samples. The values of $B_{c2}(0)$ were used to estimate the coherence lengths ($\xi(0)$) for all the samples (see Table II). The values of $B_{c2}(0)$ of our samples lie between 13 – 40 Tesla that are well within the values reported for NbN in the range ~ 13-75 Tesla.[20,21] The suppression in T_c with width in our samples can be understood by looking at the parameters obtained from the fit of the $R(T)$ curves to equation (2). From the values of k_F obtained earlier, the density of states, $N(0)$ can be estimated for all the samples by the relation,[21] $N(0)=m/\hbar^2\pi^2 k_F$, as shown in Table II. It is seen that the values of $N(0)$ for the bridge and meander samples are lower by approximately 2 order from the reported value[21] for NbN. This fall in $N(0)$ could contribute to reducing the T_c in our samples with reduced width, since $N(0)$ is directly proportional to T_c in BCS theory.

TABLE II. Sample Width, T_c, ΔT_c, Residual Resistance (RR), $B_{c2}(0)$, $\xi(0)$ and N(0) for all the samples.

Sample	Width μm	T_c K	ΔT_c K	RR (2 K) Ω	$B_{c2}(0)$ Tesla	$\xi(0)$ nm	$N(0)$ states/m_3 eV
F-NbN	1400	13.15	0.16	0	42.8	2.8	
B-NbN	50	11.63	0.4	0	35.9	3	3E+26
M-500	0.5	9.45	0.9	762	22.9	3.8	1E+27
M-250	0.25	8.36	1.3	331	16.2	4.5	8E+26
M-100	0.1	5.7	1.6	1960	12.7	5.1	6E+26

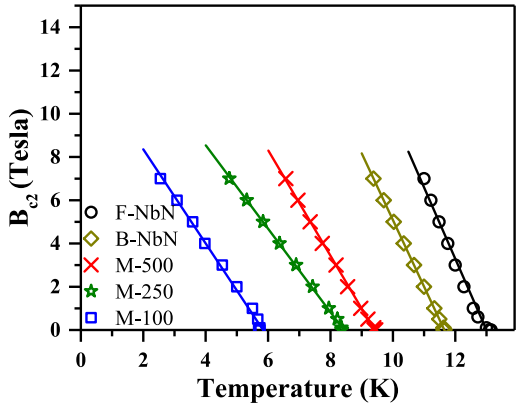

FIG. 3. Upper critical field as a function of temperature for F-NbN, B-NbN, M-500, M-250 and M-100 samples.

From Fig. 1, it is apparent that all the samples show a superconducting transition, however, zero resistance state is achieved only in case of F-NbN and B-NbN. In case of all the meanders, some residual resistance (RR) persists until the lowest measured temperature $T \sim 2$ K (see Table II). Additionally, the width of the superconducting transition ΔT, defined as the temperature difference between 10% and 90% resistance drop with respect to R_{15K}, is also seen to increase as we decrease the width of the sample (see Table II). In case of B-NbN, although the onset is similar to F-NbN, the transition is not single stepped but develops a shoulder and becomes wider with decreasing temperature. Therefore for B-NbN, the ΔT was estimated from the transition region below the shoulder. In all the meanders lower temperature resistive tails are found in addition to the broadened transition.

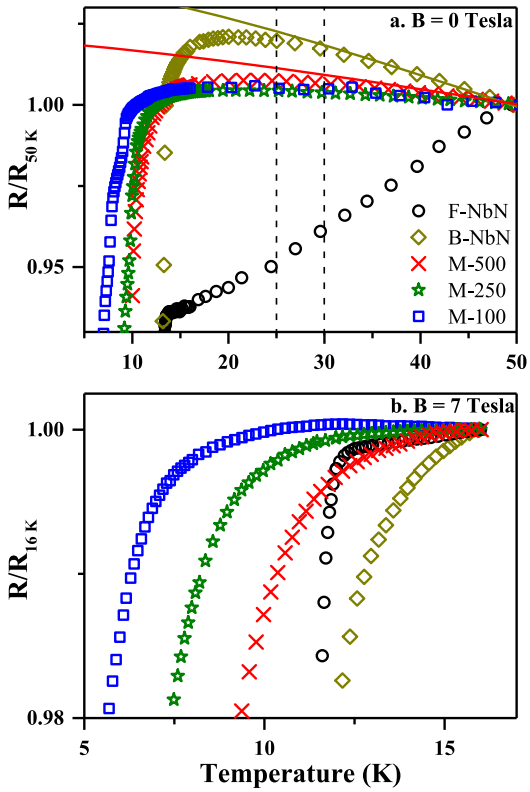

FIG. 4. Magnified graphs of R (T) curves for F-NbN, B-NbN, M-500, M-250 and M-100 samples at field (a) B = 0 Tesla, (b) B = 7 Tesla.

These results in samples with reduced width points towards the evolution of weak link effects in them.

A closer look of Fig. 2 shows excessively rounded superconducting transitions onset in case of B-NbN and meander samples in comparison to F-NbN. To check this we show in Fig. 4(a) the magnified onset of the $R(T)$ transition for all the samples at $B = 0$ Tesla, which suggests superconducting fluctuations (SFs) leading to excess conductivity in samples with reduced width.[22,23] The onset of rounding can be identified by the bifurcation point of the $R\ (T)$ curve from its normal background behavior represented by the solid lines (see Fig. 4(a)).

In F-NbN the deviation, if any, occurs at a temperature very near to T_c. In comparison, the B-NbN and meander samples show the onset of rounding at $T \sim 25$ K $>> T_c$. However, since the lowest dimension of the samples, i.e., thickness ~ 50 nm $>> \xi(0)$ (see Table I), normally excess conductivity is not expected. Thus, it seems that SFs are due to superconducting nanopaths that may have a cross-section $\leq \xi(0)^2$. The weak link effects in the bridge and meander samples as observed above may as well be a consequence of these nanopaths. Fig. 4(b) shows the magnified onset of transition for all the samples in the temperature range 2-16 K at $B = 7$ Tesla. It is clear that regardless of the increase in the magnetic field, the onset of transitions remains rounded for B-NbN and the meander samples. It is also worth noting that in case of M-100 sample the non-metallic behavior persists even in the magnetic field $B = 7$ Tesla (see Fig. 4(b)). These results show that applied magnetic field has negligible effect on the suppression of SFs and weak localization.

It can be concluded that although the normal state resistance, superconducting transition and upper critical field are found to scale with the width of the structures; the underlying cause for emergence of weak localization effects, weak link behaviour and fluctuation conductivity is fabrication induced.

IV. SUMMARY

The effect of width reduction on the transport properties of superconducting NbN nanostructures has been studied via FIB milled thin film in the form of bridge and meander samples. In the normal state, the reduced width leads to a drastic increase in the resistance and loss of metallic behavior. In the superconducting state, the width reduction results in a monotonic suppression in the T_c and B_{c2}; broader superconducting transitions; significant low temperature resistive tails; and excessively rounded superconducting onsets at $T >> T_c$. These notable changes in the normal as well as superconducting state properties of our samples with width reduction can be understood by the combined influence of size and FIB processing of our nanostructures. Our work reveals the importance of selecting the fabrication technique when engineering nanostructured superconducting devices.

ACKNOWLEDGMENTS

The authors sincerely thank the Director, CSIR-NPL, New Delhi, India for his support. LMJ and AV are grateful to Council of Scientific and Industrial Research and University Grant Commission, India, respectively, for research fellowship. The project vide Grant No. DST: SR/NM/NS-129/2010(G) is also acknowledged.

[1] A. V. Narlikar, *Frontiers in Superconducting Materials* (Springer, 2005).
[2] R. M. Scanlan, A. P. Malozemoff, and D. C. Larbalestier, "Superconducting materials for large scale applications," Proceedings of the IEEE **92**, 1639 (2004).
[3] P. Seidel, *Applied Superconductivity - Handbook on Devices and Applications* (Wiley, 2015), vol. 1 and 2.
[4] K. D. Irwin and G. C. Hilton, *Transition-Edge Sensors, in Cryogenic Particle Detection* (Springer, Heidelberg, 2005).
[5] L. Hao, J. C. Macfarlane, J. C. Gallop, D. Cox, P. Joseph-Franks, D. Hutson, J. Chen, Member, IEEE, and S. K. H. Lam, "Novel methods of fabrication and metrology of superconducting nanostructures," IEEE Trans. Instrum. Meas. **56**, 392 (2007).
[6] R. H. Hadfield, "Single-photon detectors for optical quantum information applications," Nat. Photon. **3**, 696–705 (2009).
[7] Y. Lobanov, M. Shcherbatenko, A. Semenov, V. Kovalyuk, O. Kahl, S. Ferrari, A. Korneev, R. Ozhegov, N. Kaurova, B. M. Voronov, W. H. P. Pernice, and G. N. Gol'tsman, "Superconducting nanowire single photon detector for coherent detection of weak signals," IEEE Trans. Appl. Supercond. **27**, 2200705 (2017).
[8] R. Kampwirth, D. Capone, K. Gray, and A. Vicens, "Application of NbN films to the development of very high field superconducting magnets," IEEE Trans. Magn **21**, 459–462 (1985).

[9] V. Boffa, U. Gambardella, V. Marotta, A. Morone, F. Murtas, S. Orlando, and G. P. Parisi, "NbN superconducting thin films grown by pulsed laser ablation," Appl. Surf. Sci. **106**, 361–364 (1996).
[10] E. Monticone, C. Portesi, S. Borini, E. Taralli, and M. Rajteri, "Superconducting MgB2 nanostructures fabricated by electron beam lithography," IEEE Trans. Appl. Supercond. **17**, 222 (2007).
[11] L. M. Joshi, A. Verma, P. K. Rout, M. Kaur, A. Gupta, R. C. Budhani, "The 2D–3D crossover and anisotropy of upper critical fields in Nb and NbN superconducting thin films," Physica C: Superconductivity and its applications **542**, 12 (2017).
[12] A. M. Datesman, J. C. Schultz, T. W. Cecil, C. M. Lyons, and A. W. Lichtenberger, "Gallium ion implantation into niobium thin films using a focused-ion beam," IEEE Trans. Appl. Supercond. **15**, 3524 (2005).
[13] G. C. Tettamanzi, C. I. Pakes, A. Potenza, S. Rubanov, C. H. Marrows, and S. Prawer, "Superconducting transition in Nb nanowires fabricated using focused ion beam," Nanotechnology **20**, 465302 (2009).
[14] Y. Pellan, G. Dousselin, and J. Pinei, "Temperature and magnetic field dependence of NbN film resistivity: 3D weak localization effects," J. Low Temp. Phys. **78**, 63–77 (1990).
[15] J.-H. Tyan and J. T. Lue, "Grain boundary scattering in the normal state resistivity of superconducting NbN thin films," J. Appl. Phys. **75**, 325–331 (1994).
[16] R. Baskaran and M. P. Janawadkar, "Weak localization effects in metastable superstructure niobium nitride," Mod. Phys. Lett. B **20**, 1653–1659 (2006).
[17] M. Chand, A. Mishra, Y. M. Xiong, A. Kamlapure, S. P. Chockalingam, J. Jesudasan, V. Bagwe, M. Mondal, P. W. Adams, V. Tripathi, and P. Raychaudhuri, "Temperature dependence of resistivity and Hall coefficient in strongly disordered NbN thin films," Phy Rev. B **80**, 134514 (2009).
[18] M. Kaveh and N. F. Mott, "Universal dependences of the conductivity of metallic disordered systems on temperature, magnetic field and frequency," J. Phys. C: Solid State Phys. **15**, L707–L716 (1982).
[19] V. L. Ginzburg and L. D. Landau, "On the theory of superconductivity," Zh. Eksp. Teor. Fiz. **20**, 1064–1082 (1950).
[20] M. P. Mathur, D. W. Deis, and J. R. Gavaler, "Lower critical field measurements in NbN bulk and thin films," J. Appl. Phys. **43**, 3158–3161 (1972).
[21] S. P. Chockalingam, M. Chand, J. Jesudasan, V. Tripathi, and P. Raychaudhuri, "Superconducting properties and Hall effect of epitaxial NbN thin films," Phy. Rev. B **77**, 214503 (2008).
[22] L. G. Aslamazov and A. I. Larkin, "The influence of fluctuation pairing of electrons on the conductivity of normal metal," Phys. Lett. A **26**, 238–239 (1968).
[23] W. J. Skocpol and M. Tinkham, "Fluctuations near superconducting phase transitions," Rep. Prog. Phys. **38**, 1049 (1975).